Flexible tube lattice fibers for terahertz applications

V. Setti,[1,2,*] **L. Vincetti,**[1] **and A. Argyros**[2,3]

[1] *Dipartimento di Ingegneria "Enzo Ferrari", University of Modena and Reggio Emilia, I-41125, Modena, Italy*

[2] *Institute of Photonics and Optical Science (IPOS), School of Physics, The University of Sydney, Sydney, NSW 2006, Australia*

[3] *alexander.argyros@sydney.edu.au*

[*] *valerio.setti@unimore.it*

Abstract: In this paper a flexible hollow core waveguide for the terahertz spectral range is demonstrated. Its cladding is composed of a circular arrangement of dielectric tubes surrounded by a heat-shrink jacket that allows the fiber to be flexible. Characterization of straight samples shows that the hollow core allows the absorption caused by the polymethylmethacrylate tubes of the cladding to be reduced by 31 times at 0.375 THz and 272 times at 0.828 THz with respect to the bulk material, achieving losses of 0.3 and 0.16 dB/cm respectively. Bending loss is also experimentally measured and compared to numerical results. For large bending radii bending loss scales as R_b^{-2}, whereas for small bending radii additional resonances between core and cladding appear. The transmission window bandwidth is also shown to shrink as the bending radius is reduced. An analytical model is proposed to predict and quantify both of these bending effects.

OCIS codes: (060.2400) Fiber properties; (060.2280) Fiber design and fabrication; (060.2300) Fiber measurements; (060.2430) Fibers, single-mode; (060.4005) Microstructured fibers; (300.6495) Spectroscopy, terahertz.

References and links

1. J. Anthony, R. Leonhardt, S. G. Leon-Saval, and A. Argyros, "Thz propagation in kagome hollow-core microstructured fibers," Opt. Express **19**, 18470–18478 (2011).
2. P. Doradla, C. S. Joseph, J. Kumar, and R. H. Giles, "Characterization of bending loss in hollow flexible terahertz weaveguides," Opt. Express **20**, 19176–19184 (2012).
3. A. Dupuis, K. Stoeffler, B. Ung, C. Dubois, and M. Skorobogatiy, "Transmission measurements of hollow-core thz bragg fibers," J. Opt. Soc. Am. B **28**, 896–907 (2011).
4. L. Vincetti, V. Setti, and M. Zoboli, "Terahertz tube lattice fibers with octagonal symmetry," IEEE Photon. Technol. Lett. **22**, 972–974 (2010).
5. E. Nguema, D. Fèrachou, G. Humbert, J. L. Auguste, and J. M. Blondy, "Broadband terahertz transmission within the air channel of thin-wall pipe," Opt. Lett. **36**, 1782–1784 (2011).
6. J. T. Lu, C. H. Lai, T. F. Tseng, H. Chen, Y. F. Tsai, I. J. Chen, Y. J. Hwang, H. C. Chang, and C. K. Sun, "Terahertz polarization-sensitive rectangular pipe waveguides," Opt. Express **19**, 21532–21539 (2011).
7. C. H. Lai, B. You, J. Y. Lu, T. A. Liu, J. L. Peng, C. K. Sun, and H. C. Chang, "Modal characteristics of antiresonant reflecting pipe waveguides for terahertz waveguiding," Opt. Express **18**, 309–322 (2009).
8. J. T. Lu, Y. C. Hsueh, Y. R. Huang, Y. J. Hwang, and C. K. Sun, "Bending loss of terahertz pipe waveguides," Opt. Express **18**, 26332–26338 (2010).
9. C. S. Ponseca Jr., R. Pobre, E. Estacio, N. Sarukura, A. Argyros, M. C. J. Large, and M. A. van Eijkelenborg, "Transmission of terahertz radiation using microstructured polymer optical fiber," Opt. Lett. **33**, 902–904 (2008).
10. D. S. Wu, A. Argyros, and S. G. Leon-Saval, "Reducing the size of hollow terahertz waveguides," J. Lightwave Technol. **29**, 97–103 (2011).

#180088 - $15.00 USD Received 19 Nov 2012; revised 21 Dec 2012; accepted 31 Dec 2012; published 4 Feb 2013

11. B. You, J. Y. Lu, J. H. Liou, C. P. Yu, H. Z. Chen, T. A. Liu, and J. L. Peng, "Subwavelength film sensing based on terahertz anti-resonant reflecting hollow waveguides," Opt. Express **18**, 19353–19360 (2010).
12. B. You, J. Y. Lu, C. P. Yu, T. A. Liu, and J. L. Peng, "Terahertz refractive index sensors using dielectric pipe waveguides," Opt. Express **20**, 5858–5866 (2012).
13. L. Vincetti and V. Setti, "Confinement loss in kagome and tube lattice fibers: Comparison and analysis," J. Lightwave Technol. **30**, 1470–1474 (2012).
14. F. Couny, F. Benabid, P. J. Roberts, P. S. Light, and M. G. Raymer, "Generation and photonic guidance of multi-octave optical-frequency combs," Science **318**, 1118–1121 (2007).
15. L. Vincetti and V. Setti, "Extra loss due to fano resonances in inhibited coupling fibers based on a lattice of tubes," Opt. Express **20**, 14350–14361 (2012).
16. A. Argyros and J. Pla, "Hollow-core polymer fibres with a kagome lattice: potential for transmission in the infrared," Opt. Express **15**, 7713–7719 (2007).
17. A. Argyros, S. G. Leon-Saval, J. Pla, and A. Docherty, "Antiresonance and inhibited coupling in hollow core square lattice optical fibres," Opt. Express **16**, 5642–5648 (2008).
18. Y. Y. Wang, N. V. Wheeler, F. Couny, P. J. Roberts, and F. Benabid, "Low loss broadband transmission in hypocycloid-core kagome hollow-core photonic crystal fiber," Opt. Lett. **36**, 669–671 (2011).
19. T. Grujic, B. T. Kuhlmey, A. Argyros, S. Coen, and C. M. de Sterke, "Solid-core fiber with ultra-wide bandwidth transmission window due to inhibited coupling," Opt. Express **18**, 25556–25566 (2010).
20. L. Vincetti and V. Setti, "Waveguiding mechanism in tube lattice fibers," Opt. Express **18**, 23133–23146 (2010).
21. A. D. Pryamikov, A. F. Kosolapov, V. G. Plotnichenko, and E. M. Dianov, *Transmission of CO2 Laser Radiation through Class Hollow Core Microstructured Fibers* (InTech, 2012), chap. 8, pp. 227–247.
22. G. J. Pearce, G. S. Wiederhecker, C. G. Poulton, S. Burger, , and P. S. J. Russell, "Models for guidance in kagome-structured hollow-core photonic crystal fibers," Opt. Express **15**, 12680–12685 (2007).
23. F. Gérôme, R. Jamier, J. L. Auguste, G. Humbert, and J. M. Blondy, "Simplified hollow-core photonic crystal fiber," Opt. Lett. **35**, 1157–1159 (2010).
24. A. F. Kosolapov, A. D. Pryamikov, A. S. Biriukov, V. S. Shiryaev, M. S. Astapovich, G. E. Snopatin, V. G. Plotnichenko, M. F. Churbanov, and E. M. Dianov, "Demonstration of CO_2-laser power delivery through chalcogenide-glass fiber with negative-curvature hollow core," Opt. Express **19**, 25723–25728 (2011).
25. F. Yu, W. J. Wadsworth, and J. C. Knight, "Low loss silica hollow core fibers for $3-4\ \mu m$ spectral region," Opt. Express **20**, 11153–11158 (2012).
26. Y. S. Jun, G. J. Kim, and S. G. Jeon, "Terahertz dielectric properties of polymers," J. Kor. Phys. Soc. **49**, 513–517 (2006).
27. J. Anthony, R. Leonhardt, A. Argyros, and M. C. J. Large, "Characterization of a microstructured zeonex terahertz fiber," J. Opt. Soc. Am. B **28**, 1013–1018 (2011).
28. K. Nielsen, H. K. Rasmussen, A. J. L. Adam, P. C. M. Planken, O. Bang, and P. U. Jepsen, "Bendable, low loss topas fibers for the terahertz frequency range," Opt. Express **17**, 8592–8601 (2009).
29. J. Olszewski, M. Szpulak, and W. Urbańczyk, "Effect of coupling between fundamental and cladding modes on bending losses in photonic crystal fibers," Opt. Express **13**, 6015–6022 (2005).
30. E. A. J. Marcatili and R. A. Schmeltzer, "Hollow metallic and dielectric waveguides for long distance optical transmission and lasers," Bell Syst. Tech. J. **43**, 1783–1809 (1964).
31. S. Johnson, M. Ibanescu, M. Skorobogatiy, O. Weisberg, T. Engeness, M. Soljacic, S. Jacobs, J. Joannopoulos, and Y. Fink, "Low-loss asymptotically single-mode propagation in large-core omniguide fibers," Opt. Express **9**, 748–779 (2001).
32. M. Miyagi and S. Kawakami, "Losses and phase constant changes caused by bends in the general class of hollow waveguides for the infrared," Appl. Opt. **20**, 4221–4226 (1981).
33. J. A. Stratton, *Electromagnetic Theory* (McGraw Hill, 1941). Section 9.15.

1. Introduction

Low loss, broadband and flexible waveguides are a key issue in the development of terahertz systems. Hollow core fibers have gained a lot of interest in recent years for this kind of applications [1–10] as the guiding of the electromagnetic radiation inside a hollow core is extremely helpful in reducing the propagation loss, since no highly transparent dielectrics exist at the terahertz frequencies. Moreover, having a core composed of air they allow the introduction of gases and particles for material characterization [11, 12].

Different cladding structures have been proposed for hollow core fibers in the THz spectral range, such as standalone dielectric tubes [2, 5–7] and microstructured fibers [1, 3, 9, 10]. Even though the former are very simple to manufacture, they suffer higher loss compared to a microstructured fiber with the same core size [13]. Larger core dimensions are required for

#180088 - $15.00 USD Received 19 Nov 2012; revised 21 Dec 2012; accepted 31 Dec 2012; published 4 Feb 2013

low loss but these cause many high order modes to propagate inside the hollow core [7, 10]. In order to overcome this problem, metallic coatings were proposed [2]. However complex depositions techniques are required in order to obtain very thin metallic layers so as to not affect the flexibility of the final structure. Microstructured hollow core fibers offer an interesting solution to these problems. The higher confinement of the electromagnetic radiation inside the hollow core with respect to the standalone tubes allows a smaller core size to be taken into account and it makes the guided core mode less sensitive to the surrounding environment [1, 9, 10, 14]. Differential propagation loss between the fundamental mode and the high order ones can be increased by a proper choice of cladding features, thus allowing microstructured fibers to be effectively single mode [4].

Among microstructured THz waveguides, kagome and tube lattice fibers (TLFs) have received the largest interest so far. The cladding of such fibres can be seen as composed of an array of hollow tubes with different shapes [1, 10, 13–25]. A kagome fiber for the THz range has recently been reported made from polymethylmethacrylate (PMMA) tubes [1], showing that microstructured hollow core fibers can be obtained from cheap polymers with a simple stack and draw process. Recently it was shown that circular tubes (Circular TLF, CTLF) allow better loss spectra to be obtained in terms of both minimum magnitude and transmission bandwidth when compared to kagome fibers [13, 15, 18].

In this paper a CTLF for the THz spectral range is proposed. Cladding tubes were drawn from commercially available PMMA tubes and the structure was assembled manually in such a way as to keep the waveguide flexible. These CTLF were characterized in both straight and bent configurations. In the straight configuration both dispersion and propagation loss of the fundamental core mode for the first two transmission windows were obtained. Thanks to the hollow core, the propagation loss of the fundamental core mode was strongly reduced with respect to the bulk PMMA material loss in both transmission windows. A 31 times reduction at 0.375 THz (first transmission window) and 272 times reduction at 0.828 THz (second transmission window) were obtained. The CTLF were characterized for bending loss down to bend radii (R_b) of 10 cm, and a frequency dependent bending-loss was observed for the bent fiber. A thorough numerical analysis was performed in order to investigate the properties of bent CTLF and an analytical model will be proposed in order to predict and quantify the effects of bending.

2. Manufacturing technique

Figure 1(a) shows the transverse cross section of the manufactured CTLF. The cladding is composed of a collection of eight hollow dielectric tubes placed in a circle. They have refractive index n_H, internal radius r_{int} and thickness t. The core of radius R_{co} is located in the central part of this structure and is formed by air ($n_L = 1$). The CTLF presented in this paper was manufactured from PMMA tubes with 16 mm and 12 mm external and internal diameter respectively. This tube was drawn to an external diameter of 9.6 mm using a polymer fiber drawing tower. Part of it was used for the external jacket, while the remainder was drawn again in order to obtain the cladding tubes with an average thickness of $t = 252\ \mu$m and an external diameter of about 1.99 mm ($r_{int} = 743\ \mu$m). The final core radius was $R_{co} = 1.62$ mm. The cladding tubes were cut into pieces 10 cm and 20 cm long.

In order to realize a flexible THz fiber, the external jacket tube was cut into small pieces 5 mm in length. These are necessary to keep the cladding tubes in place, but at the same time they have to be separated from each other in order to make the fiber flexible. Therefore the cladding tubes were manually stacked inside these jacket rings, and the rings were spaced 10 cm apart forming a self supporting structure. No glue or fusing was necessary to keep the components in place. An external heat-shrink jacket was added over the entire structure to enhance its mechanical stability during the bending. Figure 1(b) gives a side picture of the fiber

#180088 - $15.00 USD Received 19 Nov 2012; revised 21 Dec 2012; accepted 31 Dec 2012; published 4 Feb 2013

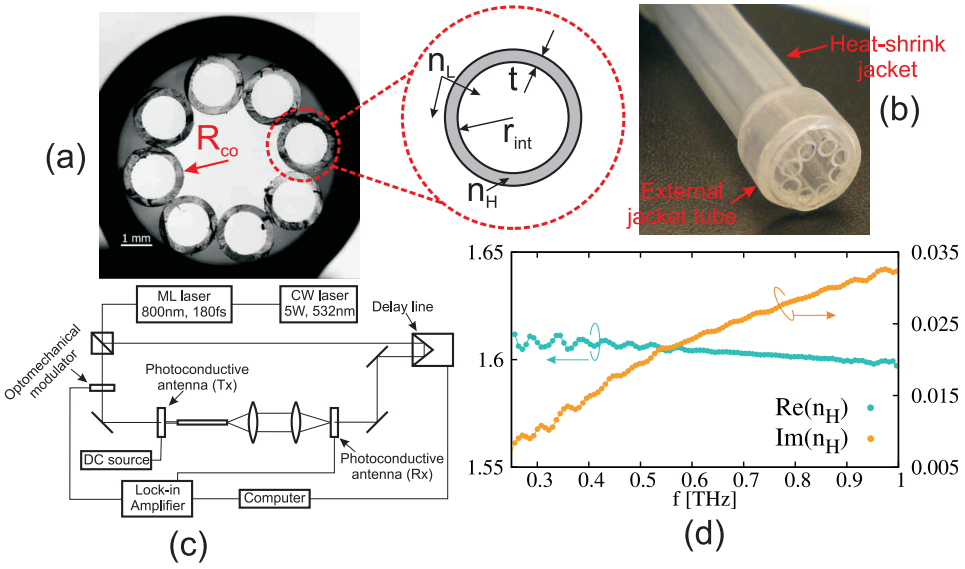

Fig. 1. (a) Microscope image of the transverse cross section of the manufactured fiber along with its physical dimensions and dielectric properties. (b) Side picture of the fiber. (c) THz-TDS setup that have been used to characterize the straight fiber. (e) Frequency dependence of $\Re(n_H)$ and $\Im(n_H)$ measured experimentally for a PMMA disk.

in order to show the final cladding shape. In order to give a reliable comparison between the experimental results and the simulations a 2 mm thick PMMA disk was characterized via THz time domain spectroscopy. Figure 1(d) shows the measured real, $\Re(n_H^{PMMA})$, and imaginary, $\Im(n_H^{PMMA})$, of the PMMA refractive index in the range $[0.25;1]$ THz. As expected $\Re(n_H)$ was almost constant in the frequency range of interest, while $\Im(n_H)$ changes with frequency [26].

3. Absorption and confinement loss in CTLFs

The characterization of the fibre in a straight configuration was done using the THz time domain spectroscopy (THz-TDS) setup shown in Fig. 1(c). THz-TDS is widely used for the analysis of THz waveguides as it gives both phase and magnitude information for the detected radiation. Measurements on fibers of different length can be easily performed by moving only the first lens after the fiber's output, such that the output remains in its focal plane. Dispersion curves were computed by comparing the phase of a pulse propagating through free space to that propagating through the fiber. In a similar way, propagation loss was computed by comparing the spectral magnitude of two fibers of different length, thus avoiding problems associated with estimating the coupling efficiency for the fibers. Great attention was paid to the positioning of the lenses and the waveguides and multiple scans were performed in order to maximize the received power over the entire spectrum and minimize any misalignment. Moreover, integration times as long as 3 s were used for the scans in order to minimize noise in the received signal.

For comparison, all the experimentally measured properties of the fibres and PMMA reported in the previous section were used to generate a model of the manufactured CTLF in a finite element software package (Comsol Multiphysics). For simplicity the jacket was approximated with a hollow pipe surrounding the cladding tubes, with thickness $3t$ and refractive index equal to that of PMMA.

Figure 2(a) compares the simulation and experimental results for the effective mode index

#180088 - $15.00 USD Received 19 Nov 2012; revised 21 Dec 2012; accepted 31 Dec 2012; published 4 Feb 2013

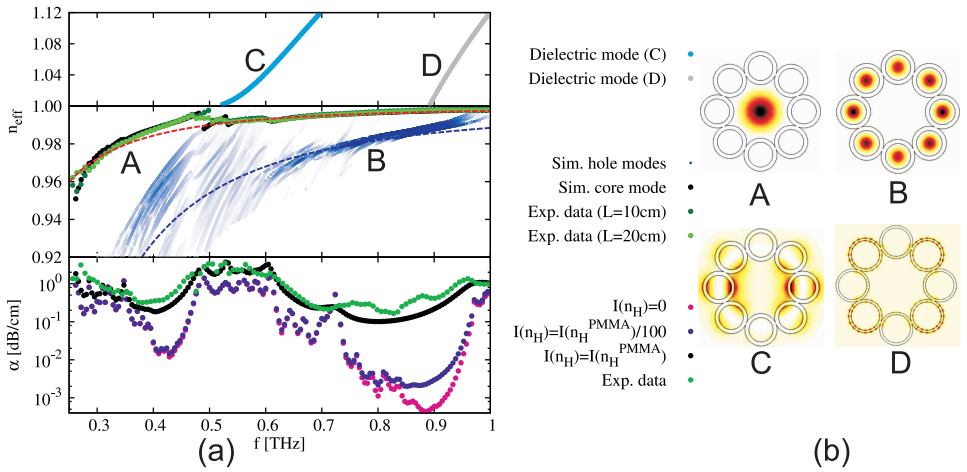

Fig. 2. (a) Top and middle panels show the numerical dispersion curves for two dielectric modes with different periodicity along the transverse direction, the core mode and hole modes. For the hole modes the color intensity is proportional to the power inside the hole regions normalized with respect to the total power of the mode. Experimental data is also shown. Bottom panel shows numerical propagation loss for the core mode with different values of $\Im(n_H)$ and also experimentally measured loss. (c) Example images for the three different classes of modes supported by the waveguide.

(n_{eff}) and loss in the frequency range $[0.25;1]$ THz and an overall excellent agreement is found for both. Two transmission windows were observed, the fundamental (lowest frequency) one extending from 0.29 THz to 0.47 THz, and the second one extending from 0.61 THz to 0.95 THz. High loss peaks separate the different transmission windows. These peaks are due to the coupling between the core mode (labelled A in Fig. 2(b)) and the lower order dielectric modes which are confined to the high index (solid) part of the cladding tubes (labelled C in Fig. 2(b)). This coupling occurs when the two are resonant, as seen in Fig. 2(a), which occurs for frequencies satisfying [14–17, 19–22]:

$$f_{Rm} = \frac{mc}{2t\sqrt{\bar{n}_H^2 - n_L^2}}, \qquad m \in \mathbb{N}, \tag{1}$$

where c is the speed of light in vacuum and $\bar{n}_H = 1.6$ is the mean value of n_H. High order dielectric modes, such as D in Fig. 2(b), do not result in such loss peaks [16, 20].

The propagation loss of the guided mode is strongly reduced with respect to the bulk materia absorption loss due to the hollow core [16]. Comparing the experimentally measured loss of the CTLF and the material absorption of the PMMA, a reduction of 31 times ($\alpha = 0.3$ dB/cm) at 0.375 THz and 272 times (0.16 dB/cm) at $f = 0.828$ THz were obtained, with these frequencies corresponding to the approximate centres of the two transmission windows as seen in Fig. 2(a). This confirms that the guided mode is confined in the hollow core of the fiber and also that hollow-core waveguides such as CTLFs are potentially low loss waveguides for the terahertz range. Materials with lower absorption such as Zeonex [27] or Topas [28] would reduce the propagation loss of the guided core mode even further.

Figure 2(a) shows the effect of the cladding tubes' absorption on the propagation loss of the core mode. PMMA tubes are compared with ideal lossless tubes and highly transparent ones. The latter represent a generic low loss THz material, such as Zeonex or Topas, with an imaginary part of the refractive index about a hundred times lower than PMMA [27, 28].

#180088 - $15.00 USD Received 19 Nov 2012; revised 21 Dec 2012; accepted 31 Dec 2012; published 4 Feb 2013

In the first transmission window, the difference of more than an order of magnitude between PMMA and lossless tubes shows that PMMA absorption dominates the loss. On the contrary in the case of low loss tubes, the absorption is negligible. In the second transmission window, by using low loss tubes instead of PMMA, a reduction of about two orders of magnitude is obtainable. However, the additional loss obtained from the low-loss tubes compared to the lossless tubes is no longer negligible. Overall, this analysis shows that although the absolute value of loss is higher in the first transmission window, the effects of absorption in the cladding tubes are more severe in the second transmission window. Even though these highly transparent polymers would allow a further reduction of the propagation loss, the purpose of this paper is not to optimize transmission. The goal is to investigate the potential of CTLFs in reducing the absorption caused by the dielectric material of the cladding and their bending loss properties.

As shown in Fig. 2(b), CTLFs also support hole modes (labelled B). The core mode and the hole modes are both confined in hollow regions and have dispersion values that lie below the air line. Far from resonances with dielectric modes their dispersion curves can be approximated by:

$$n_{eff} = n_L - \frac{1}{2}\left(\frac{u_{\nu\mu}c}{2\pi f R\sqrt{n_L}}\right)^2 \tag{2}$$

which is an extension of the Marcatili's formula as shown in the appendix, where $u_{\nu\mu}$ is the μ-th zero of the Bessel function $J_\nu(u)$. R is the radius of the hollow core waveguide under analysis, that is $R = R_{co}$ and $R = r_{int}$ for the core and hole modes respectively. Since $R_{co} > r_{int}$, Marcatili's dispersion curves of the core and hole modes never intersect. As shown in Fig. 2(a), there are some frequencies where dispersion curves of hole modes separate form their Marcatili's approximation, due to anticrossings between hole and dielectric modes. In these regions hybridized modes appear, however the power rapidly shifts from the hole to the dielectric modes. Therefore hole modes are never phase matched with the fundamental core one, thus they do not contribute to the confinement mechanism of the latter. However, it has been shown in the literature that they can been exploited to increase the differential loss between the fundamental core mode and higher order modes [4]. Moreover they can cause additional resonances and extra losses in the case of fibre bending [21, 23, 24].

4. Bending loss

The 20 cm long CTLF sample was used for the bend-loss characterization, and a schematic and a photograph of the experiment are shown in Figs. 3(a,b). The setup is basically identical to that used for the characterization of the straight fiber, however the THz path was changed to accommodate for the bent fibre. The CTLF's input remained adjacent to the transmitter antenna, but the output was shifted in order to achieve the desired bending radius R_b. Two mirrors were used to redirect the output beam to the receiver. Figure 3(b) shows the experimental setup in the case of a bending radius $R_b = 10$ cm, roughly corresponding to a 90° bend. Two clamps were used to hold the ends of the fibre, thus limiting the actual bendable length of the fiber to 16 cm.

Figure 3(c) shows that in both transmission windows the low frequency edges are substantially insensitive to bending, whereas the high frequency edges shift toward lower frequencies as R_b decreases. As already observed in other inhibited coupling fibers, the first transmission window is less sensitive to the bending than the high order ones [23,25]. In the first transmission window, $R_b = 10$ cm is required to observe a clear shift of the high frequency edge, whereas in the second window the shift is apparent with $R_b = 30$ cm. Apart from the high frequency edge shift at $R_b = 10$ cm, the normalized transmission in the first window is otherwise unaffected by the bending. The second window, on the contrary, is more sensitive. When $R_b = 30$ cm the normalized transmission separates from the straight case only for $f > 0.85$ THz. A reduction of

#180088 - $15.00 USD Received 19 Nov 2012; revised 21 Dec 2012; accepted 31 Dec 2012; published 4 Feb 2013

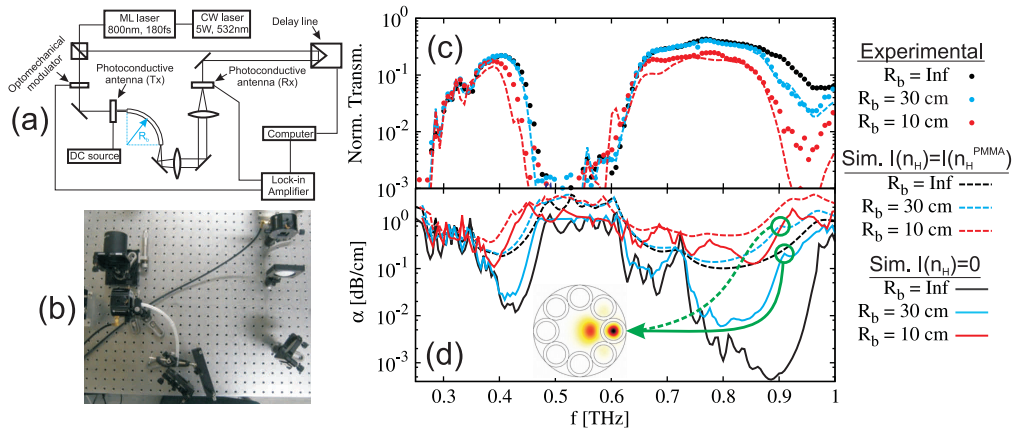

Fig. 3. (a) THz-TDS setup that have been used to characterize the 20 cm fiber sample for the bending. (b) A picture of the setup. (c) Experimental and numerical normalized transmission of the 20 cm TLF sample for different bending radii. (d) Comparison of propagation loss in case of bending for CTLFs with transparent and PMMA tubes.

the bending radius down to 10 cm causes a decrease in transmission over essentially the entire transmission window.

4.1. Analysis of the bending loss

The numerical analysis of the bending loss performed in this paper is based on the conformal mapping technique [29], where a bent fiber with refractive index $n(x,y)$ is analyzed in terms of a straight fiber with a refractive index:

$$\tilde{n}(x,y) = n(x,y)e^{\xi/R_b}. \tag{3}$$

In this expression, $\xi = \{x,y\}$ is the bending direction while R_b is the bending radius. A schematic of this effect is shown in Fig. 4(a) for bending in the *xz* plane, but the same can be readily applied also for a bending in the *yz* plane.

First of all the transmission spectra for $R_b = \{10,30,\infty\}$ cm were computed and compared with experimental results in Fig. 3(c), observing a good agreement and confirming the validity of the numerical analysis. In order to better understand the loss mechanisms in bent CTLFs and to separate the effects of the leakage and of the material absorption, the propagation loss spectra with $R_b = \{10,30,\infty\}$ of CTLFs with PMMA and lossless tubes were computed and are shown in Fig. 3(d). As expected, the lossless case is more sensitive to bending because the loss of the straight fiber is much lower than in the absorbing case. However, it is important to point out that the shift of the high frequency edges exist in both cases, thus it is due to confinement mechanisms and not to material absorption. In addition extra peaks inside the transmission windows are observed as highlighted and shown in the inset of Fig. 3(d). They are due to extra resonances between the core mode and hole modes as already observed in other inhibited coupling fibers [21, 23, 24]. Their spectral position strongly depends on the bending radius. This is clearly shown in Fig. 4(c) where the calculated propagation loss spectrum in the second transmission window is shown for decreasing values of R_b (from 30 cm to 18 cm). When R_b falls below 30 cm, this new resonance shifts toward lower frequencies, thus compromising that transmission window.

These results show that bending loss in CTLFs even with highly absorbing materials does not only depend on the material absorption, but also on the waveguiding mechanism. These

#180088 - $15.00 USD Received 19 Nov 2012; revised 21 Dec 2012; accepted 31 Dec 2012; published 4 Feb 2013

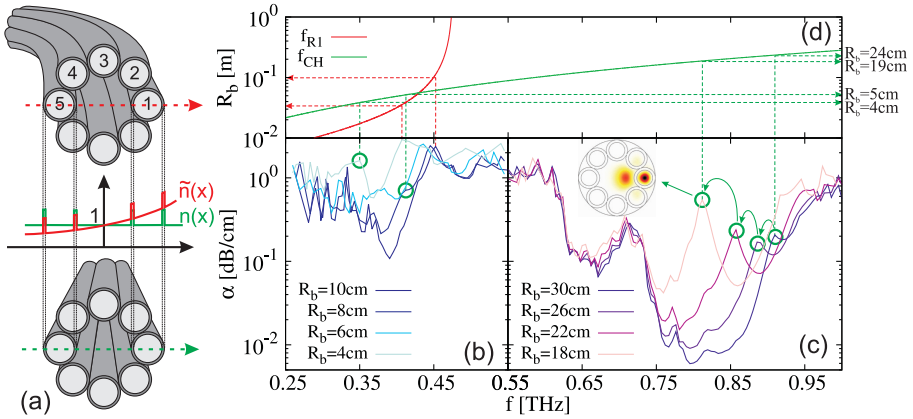

Fig. 4. (a) Effect of the conformal mapping on the refractive index of the fiber in the transverse direction. (b) Propagation loss of the core mode in the first transmission window for $R_b = \{4, 6, 8, 10\}$ cm (from light to dark blue). (c) Propagation loss of the core mode in the second transmission window for $R_b = \{18, 22, 26, 30\}$ cm (from light to dark violet). The resonance between core and hole mode is highlighted in the inset. (d) Evaluation of Eq. (4) for the first resonance edge (red) and of Eq. (5) for the resonances between core and hole modes (green) in the two transmission windows.

aspects are analyzed in depth in the next section.

5. Analytical models for bending loss in CTLFs

In the previous section it was shown that in bent CTLFs the reduction of the transmission window bandwidth and the loss due to extra resonances arose from the waveguiding mechanism and not the material absorption. Although some results on the behavior of bent inhibited coupling fibers already exist for the infrared spectral region [21, 23–25], due to their experimental or strictly numerical nature they are unable to provide a deep insight into underlying physical mechanism that affects the fibers in the case of bending. For this reasons, in the next sections a thorough numerical and theoretical analysis based on the conformal mapping technique will be presented.

5.1. High frequency edge shift

As shown in Fig. 4(a) the bending causes an increment of the refractive index of the outer tubes (relative to the bend), and therefore a change of the dispersion characteristics of both dielectric and hole modes. The shift of the high frequency transmission window edges is due to the shift of the cut-off frequencies of the dielectric modes. By substituting Eq. (3) in Eq. (1) it is possible to estimate the new position of the edges due to the bending:

$$f'_{Rm} = \frac{mc}{2t\sqrt{(\bar{n}_H e^{\hat{x}/R_b})^2 - n_L^2}} \tag{4}$$

where $\hat{x}$ represents the coordinate of the outermost part of the tube on the right side of the structure in Fig. 4(a), $\hat{x} = R_{co} + 2(r_{int} + t)$. This substitution causes the denominator in Eq. (4) to increase relative to Eq. (1), and hence f'_{Rm} decreases. The bending radius required to shift the high frequency edge of the first transmission window to a particular frequency as calculated by Eq. (4) is shown in Fig. 4(d) (red curve).

#180088 - $15.00 USD Received 19 Nov 2012; revised 21 Dec 2012; accepted 31 Dec 2012; published 4 Feb 2013

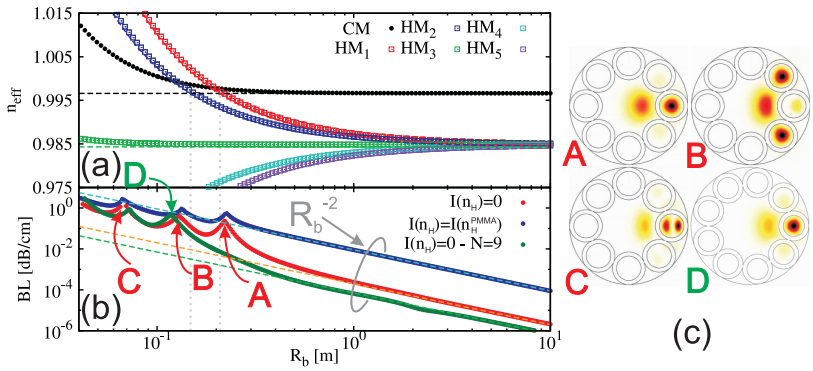

Fig. 5. (a) Numerical (dots) and analytical (dashed lines) effective indices for the hole modes and the core mode of the CTLF. (b) Bending loss for CTLFs with 8 (red dots) and 9 (green dots) transparent cladding tubes and for a 8 PMMA tubes CTLF (blue) at 0.86 THz. Dashed lines represent the asymptotic R_b^{-2} trend. (c) Poynting vector intensities for the core mode at the high loss peaks reported in (b).

Figures 4(b) and 4(d) allow a comparison of the numerical results with those predicted by Eq. (4) for the high frequency edge of the first transmission window. Excellent agreement is found. For large bending radii, the shift is negligible, as indicated by the increasing, steep gradient above 0.45 THz (Fig. 4(b), red curve). By reducing R_b the edge shifts quicker, limiting the transmission window bandwidths.

5.2. Extra loss due to hole modes resonances

The extra loss due to the resonances between the core mode and hole modes appear when the modes are phase matched. In a straight fiber this cannot happen because of the different size between the fiber core and the cladding holes. However, Fig. 4(a) shows that due to the conformal mapping on the bent fiber, the refractive indices inside the cladding holes change according to their relative position along the bending direction and the bending radius. In particular, the effective indices of the modes of the outer tubes increase approaching the effective index of the core mode until the phase matching condition is reached, causing the extra losses.

By assuming a uniform refractive index inside each hole for simplicity, and by substituting the values $\tilde{n}_L(x_{ci},y_{ci})$ in Eq. (2), it is possible to analytically describe the effective index of the holes modes of the i-th tube centered at (x_i,y_i) for the bent fiber. In Fig. 5(a) the analytical curves of the effective indices of the core and hole modes at $f = 0.86$ THz are shown as a function of the bending radius. They are compared with the numerical curves obtained by applying the conformal mapping technique to a single hole with internal radius r_{int}, refractive index $n_L = 1$, centered at (x_{ci},y_{ci}) and immersed in an infinite dielectric medium with refractive index $\Re(n_H) = \Re(n_H^{PMMA})$ and $\Im(n_H) = 0$. A good agreement is found showing the validity of the proposed analytical model. Small discrepancies appear only for the hole mode placed on the y axis (hole 3 in Fig. 4(a)) because for tight bends, the hole mode field profile shifts toward the outer part of the bending plane whereas the analytical model neglects this distortion. The same observations can be made for the effective index of the core mode. The difference between analytical and numerical results appears for larger bending radii for the core mode compared to hole 3 mode because having $R_{co} > r_{int}$ the field profile bending distortion is more pronounced for the core mode than the hole mode, as shown in Fig. 5 (c). The crossing points between the core mode and hole mode curves in Fig. 5(a) represent the phase matching conditions, that is the resonances between core and holes modes. By equating Eq. (2) for both the core and the

#180088 - $15.00 USD Received 19 Nov 2012; revised 21 Dec 2012; accepted 31 Dec 2012; published 4 Feb 2013

mode of a hole positioned at $x = x_c$ it is possible to have an analytical estimation of the bending radii at which these resonances appear:

$$R_b = \frac{x_c}{\ln\left[\frac{M(R_{co})}{2} + \sqrt{\left(\frac{M(R_{co})}{2}\right)^2 - M(r_{int}) + 1}\right]}, \qquad M(R) = 1 - \frac{1}{2}\left(\frac{u_{nm}c}{2\pi f R}\right)^2. \tag{5}$$

The resonance with the outermost hole mode defines the tolerance of the CTLF to additional high loss peaks. The green curve in Fig. 4(d) shows the evaluation of Eq. (5) with $x_c = x_{c1}$ over the first two transmission windows, whereby the bending radius required to shift the resonance between the core and the mode of hole 1 to a particular frequency is plotted as a function of frequency. No resonances are found in the first two transmission windows for $R_b > 30$ cm meaning that the considered CTLF is relatively robust against extra resonances for such bending radii. However, when R_b falls below this, the resonance appears in the second transmission window and shifts toward lower frequencies, eventually reaching the first transmission window at $R_b \approx 5$ cm.

Figure 5(b) shows also the bending loss ($BL(R_b) = \alpha(R_b) - \alpha(\infty)$) at $f = 0.86$ THz versus the bending radius. For large bending radii BL increases as $1/R_b^2$ as it has already been reported in the literature for other hollow core waveguides [30–32]. For small value of R_b, many additional loss peaks appear due to the resonances with hole modes. The intensity profile of the core mode at these peaks is shown in Fig. 5(c). The R_b values of the extra losses are well predicted by Eq. (5). Figure 5(b) shows also the bending loss for the core mode of a CTLF with PMMA cladding tubes. For large R_b values the bending loss still scales as R_b^{-2} as was found for the lossless case. The higher magnitude of bending loss with respect to the ideal case can be ascribed to the additional loss caused by PMMA absorption in the bent fiber. Extra losses due to the resonances between the core and hole modes are still present and their position is not changed with respect to the ideal tubes. However, their relative magnitude with respect to the background bending loss is reduced because the loss is already higher due to material absorption. For this reason it was not possible to clearly identify such extra resonance on the experimental normalized transmission graphs reported on Fig. 3(c).

In order to further confirm the proposed model, Fig. 5(b) shows also the bending loss for a CTLF of an alternative design with nine tubes in the cladding. In this case, R_{co} and t remain the same as before, and r_{int} is reduced to 596 μm, with a schematic shown in the lower right panel of Fig. 5(c). According to Eq. (2), this change causes a reduction of the effective index for the hole modes in the straight fiber, whereas the core mode is unaffected. As a consequence a smaller bending radius is necessary to reach the phase matching condition between core and hole modes. Numerical results shown in Fig. 5(b) confirm that the first resonance shifts toward lower values of bending radius, and allows the bending radius to be further reduced by 10 cm before such resonances appear. This provides an avenue for increasing the amount of bending possible before such resonances affect the transmission.

6. Conclusions

In this paper a flexible circular tube lattice fiber for THz applications has been demonstrated and investigated numerically and experimentally. The cladding was made from widely available polymethylmethacrylate tubes displaced circularly around a hollow core. The structure was assembled manually without the need of further drawing steps or glue. A heat-shrink jacket was added to enhance the mechanical stability of the structure while keeping it flexible.

Samples of different lengths were used to characterize the dispersion and propagation loss for the manufactured fibers. An excellent agreement with the numerical results was found:

#180088 - $15.00 USD Received 19 Nov 2012; revised 21 Dec 2012; accepted 31 Dec 2012; published 4 Feb 2013

propagation loss was reduced by 31 times at 0.375 THz and 272 times at 0.828 THz with respect to the bulk material, these frequencies corresponding roughly to the centre of the two observed transmission windows. At these frequencies the overall measured loss was 0.3 dB/cm and 0.16 dB/cm. Through a numerical analysis it was shown that propagation loss can be greatly reduced if a material with lower absorption (e.g. Zeonex, Topas) is used for the cladding tubes.

The 20 cm sample was used to characterize the bending. The lower frequency transmission window showed to be the most robust against bending and a bending radius as low as $R_b = 10$ cm was necessary to produce a clear reduction in the transmission spectrum. A higher sensitivity was found for the second transmission window: here a $R_b = 30$ cm produced visible perturbations to the transmitted spectrum.

A thorough numerical analysis of the bending in CTLFs was also performed in order to investigate all the effects that limit the performance in such bent waveguides. In general, due to the bending, there is an expansion toward lower frequencies of the high loss peaks that delimit the transmission windows. An analytical formula was proposed to estimate the amount of this shifting as a function of the bending radius. However, bending radii as small as $R_b < 20$ cm are required in order to have a visible reduction of the transmission bandwidth for the first and the second transmission window.

Taking into account a single frequency for the bending analysis, it was found that for large values of R_b, bending loss scales as R_b^{-2}. On the contrary, for small bending radii additional resonances between core and various hole modes were found. These cause extra loss peaks in the propagation loss of the core mode. An analytical model was proposed in order to predict the bending radius at which these resonance appear once the working frequency is defined. A good agreement was found between the analytical formula and the numerical data, showing that this model can be used to determine the bending tolerance of CTLF to these extra resonances. It was shown that these resonances appear only for $R_b < 30$ cm (for the second transmission window), therefore making CTLF relatively immune to them. In order to further test the proposed analytical model, a CTLF with nine tubes in the cladding was also considered. As expected the first resonance between core and hole modes shifted toward smaller bending radii, allowing the waveguide to become more insensitive to these extra resonances.

A. Marcatili's formula for solid core tube fibers

Marcatili's formula has been widely used in the literature to describe the dispersion properties of the core mode of hollow core waveguides [20, 30]. The main limitation of this formula is that it was developed assuming that the core is made of air ($n_L = n_{air} = 1$). In this appendix Marcatili's formula is extended to take into account also hollow core waveguides with a generic refractive index core.

Consider a circular waveguide of radius R and refractive index n_L embedded in an another dielectric medium of infinite extent and refractive index n_H. Here, for simplicity, both n_H and n_L are real and $n_L < n_H$. Owing to the geometry of the problem, a cylindrical coordinate system is assumed. Two propagation constants, K_τ ($\tau = \{L, H\}$) and β, can be defined: the former is directed along the transverse plane of the waveguide, while the latter along the axial one. These two constants satisfy the relation $K_0^2 n_\tau^2 = K_\tau^2 + \beta^2$, where $K_0 = 2\pi f/c$ is the propagation constant in free space. With these assumptions, it can be shown that the dispersion relation for the modes guided inside the internal cylinder satisfies [33]:

$$\left[\frac{J_\nu'(K_L R)}{J_\nu(K_L R)} - \frac{K_L}{K_H}\frac{H_\nu^{(1)\prime}(K_H R)}{H_\nu^{(1)}(K_H R)}\right]\left[\frac{J_\nu'(K_L R)}{J_\nu(K_L R)} - \frac{K_L}{K_H}\frac{n_H^2}{n_L^2}\frac{H_\nu^{(1)\prime}(K_H R)}{H_\nu^{(1)}(K_H R)}\right] = \left[\frac{\nu\beta}{K_L^2 R^2}\left(\frac{K_L^2}{K_H^2} - 1\right)\right]^2, \tag{6}$$

where $J_\nu(x)$ and $H_\nu^{(1)}(x)$ are the Bessel and Hankel functions of the first kind. Solving Eq.

#180088 - $15.00 USD Received 19 Nov 2012; revised 21 Dec 2012; accepted 31 Dec 2012; published 4 Feb 2013

(6) means finding the propagation constants β of the guided modes. Two hypotheses can now be introduced to simplify calculations: first, the core radius is much bigger than the working wavelength (i.e. $K_0R >> 1$) and, second, modes guided inside the internal cylinder have a propagation constant which is very close to that of the bulk material (i.e. $\beta \approx K_0 n_L$). Neglecting all powers of K_L/K_H greater than one, and introducing the following approximation:

$$\frac{H_\nu^{(1)\prime}(K_H R)}{H_\nu^{(1)}(K_H R)} \approx i, \tag{7}$$

it is possible to reduce Eq. (6) to the following form:

$$J_{\nu-1}(K_L R) = i \frac{\eta}{\sqrt{(\frac{n_H}{n_L})^2 - 1}} \frac{K_L}{K_0 n_L} J_\nu(K_L R), \tag{8}$$

where:

$$\eta = \begin{cases} \frac{1}{2}\left[1 + (\frac{n_H}{n_L})^2\right] & \text{for } HE_{\nu\mu} \text{ and } EH_{\nu\mu} \text{ modes} \\ 1 & \text{for } TE_{0\mu} \text{ modes} \\ (\frac{n_H}{n_L})^2 & \text{for } TM_{0\mu} \text{ modes} \end{cases} \tag{9}$$

Under the assumptions already made, the term on the right hand side of Eq. (8) is in general small. Therefore, a perturbation technique can be applied to solve Eq. (8) keeping only the first term of the perturbation obtaining [30]:

$$K_L \approx \frac{u_{\nu\mu}}{R}\left[1 - i\nu \frac{1}{K_0 n_L R} \frac{\eta}{\sqrt{(\frac{n_H}{n_L})^2 - 1}}\right], \tag{10}$$

where $u_{\nu,\mu}$ is the μ-th zero of the function $J_{\nu-1}(x)$. It is now straightforward to obtain propagation constants for the guided modes:

$$\beta = Re\left\{\sqrt{K_0^2 n_L^2 - K_L^2}\right\} \approx \frac{2\pi f}{c} n_L \left[1 - \frac{1}{2}\left(\frac{u_{\nu\mu} c}{2\pi f R n_L}\right)^2\right], \tag{11}$$

and then finally

$$n_{eff} = \frac{\beta}{K_0} = n_L - \frac{1}{2}\left(\frac{u_{\nu\mu} c}{2\pi f R \sqrt{n_L}}\right)^2. \tag{12}$$

Acknowledgments

A. A. is supported by an Australian Research Council Australian Research Fellowship. This work was performed in part at the OptoFab node of the Australian National Fabrication Facility, a company established under the National Collaborative Research Infrastructure Strategy to provide nanofabrication and microfabrication facilities for Australian researchers. The authors thank R. Lwin for assistance with the fiber fabrication, and J. Anthony and R. Leonhardt for advice and assistance with components for the THz-TDS measurements.

#180088 - $15.00 USD Received 19 Nov 2012; revised 21 Dec 2012; accepted 31 Dec 2012; published 4 Feb 2013